ARTICLE

Materials and Corrosion

Depassivation and repassivation of stainless steels by stepwise pH change

Emir Mujanović | Bojan Zajec[1] | Andraž Legat[1] | Tadeja Kosec[1] |
Janez Kovač[2] | Gregor Mori[3] | Stefan Hönig[4] | Gerald Zehethofer[4]

[1]Laboratory for Metals, Corrosion and Corrosion Protection, Slovenian National Building and Civil Engineering Institute, Ljubljana, Slovenia

[2]Department of Surface Engineering and Optoelectronics, Jožef Stefan Institute, Ljubljana, Slovenia

[3]Department of General, Analytical and Physical Chemistry, Montanuniversitaet Leoben, Leoben, Austria

[4]Laboratory for Exploration and Production, OMV Exploration & Production GmbH, Gänserndorf, Austria

Correspondence
Gregor Mori, Department of General, Analytical and Physical Chemistry, Montanuniversitaet Leoben, Franz-Josef-Strasse 18, A-8700 Leoben, Austria.
Email: mori@unileoben.ac.at

Abstract

Immersion tests with different stainless steels have been performed, while the pH was stepwise decreased and then increased again. During 8.5-day exposure, the depassivation and repassivation pH values as a function of pitting resistance equivalent number were determined. There is always a gap between both pH values (depassivation and repassivation), indicating that for every steel, there are conditions where an existing passive layer can be maintained but cannot be rebuilt after depassivation. In such environments, the passive layer is thicker, consisting mainly of molybdenum and iron rich oxides, while chromium is dissolved. Usually, depending on conditions, the passive layer is more chromium-rich, especially the inner layer. This is relevant, for example, for acidizing jobs in oil and gas industry, proving that repassivation after acidizing will happen promptly, when the pH is increased again.

KEYWORDS
depassivation, passivity, repassivation, stainless steels

1 | INTRODUCTION

Steels containing at least 10.5% of chromium are considered stainless steels. This is due to the layer formed on such steels, containing chromium and/or iron oxyhydroxides. A passive layer greatly slows down oxidation and protects the underlying metal from corrosion.[1] It is widely accepted that the protectiveness of the passive layer depends on its thickness and the defect density in the layer.

The passive layer can be divided into the "outer" and "inner" part of the film. The steel underneath the passive layer can also be divided into the bulk metal deep in the metal part and the underlying metal found just underneath the passive film, which is often named as interface.[2] Usually, the interface is rich in nickel and nitrogen; however, this may vary depending on the conditions in which the passive film is formed. The passive layer is rich in alloying elements less noble than iron, mainly Cr and Mo, in case of CrMnN austenitic steels, also in Mn. Passive layers formed on stainless steel have an average thickness between 1 and 4 nm. The presence of Cl^- ions in an environment will cause the native oxide layer to be thinner.[3]

In neutral and alkaline pH solutions, both iron and chromium oxyhydroxides are found on the surface of the passive layer, whereas in low pH solutions, the passive film/electrolyte interface is strongly enriched with chromium as iron is dissolved.[4] If the pH is reduced even further, to values near 3 or below, very little chromium

shall be found on the surface of the film, and an enrichment in iron oxyhydroxides should take place according to Pourbaix diagrams.[5] Although Pourbaix diagrams of pure metals only represent thermodynamics and do not consider mixed oxide formation, such as spinels or metastable oxide formation, one can derive a coarse tendency of what might be expected from metals and sometimes even alloys (by looking at the right diagrams) with respect to their corrosion and possible passivation behavior. When the pH decreases below 3.7, chromium is stable as a divalent or trivalent ion and dissolves. At very high potentials close to and above oxygen formation, the hexavalent chromate ion is stable. Due to this reason, stainless steels show a so-called secondary passivity at very high potentials, where trivalent chromium hydroxide from the passive layer is dissolved in chromate ions. At this elevated potential range, the iron hydroxide is still stable and protects the steel. Due to its higher defect order, the protective effect of pure iron oxide/hydroxide is lower than the one for chromium oxide/hydroxide. This will result in secondary passivity, which can be derived from Pourbaix diagrams and that is experimentally found especially in sulfuric acid electrolytes.[6] The secondary passivity always shows a higher corrosion current density than the true passivity, where both metal oxides/hydroxides are contributing to passivity, as the defect density of iron oxide/hydroxide is higher than that of chromium oxide/hydroxide or of the combined oxide/hydroxide.

There are different ways of depassivation of stainless steels. Localized depassivation can either happen chemically by chloride ions introducing pits or mechanically during the impact of hard particles, by wear or by scratching. Among a vast number of publications and books on pitting (and crevice) corrosion by Szklarska-Smialowska,[7] there are a large number of reviews on pitting and depassivation by chloride ions in earlier[8-10] and in more recent years.[11-13] We have recently reported our investigations on early stages of mechanical depassivation by scratch tests,[14,15] along with a comprehensive literature review on mechanical depassivation.[15] We have shown that after mechanical depassivation in scratch tests on various stainless steels, repassivation at open circuit potential takes place within the first few tenths of a second after scratching; however, final healing of the passive layer and reaching a steady passive state take much longer. These results are in accordance with other researchers.[16-21] Whereas early repassivation in many media occurs between a few tenths of a second and some seconds and reaches a passive current density in the range between 0.1 and 1 mA/cm², Burstein and Daymond[22] have shown that 316-L stainless steel in 0.1-M H_2SO_4 at 300 mV_{SCE} reaches a passive current density of 16 nA/cm² within 15 h. When applying nine temperature cycles between 20°C and 85°C for another 11 h, passive current density dropped to as low as 0.5 nA/cm². The authors concluded that even at these values, the passive current density probably continues to decrease further, so that a true steady-state passivity is still not reached.
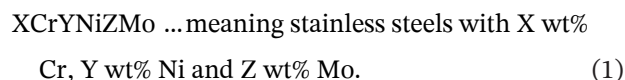
The other form of depassivation (besided localized depassivation) is general depassivation, which occurs when the environmental conditions are too aggressive for the passive layer to persist. In the case of oil production, this usually occurs during acidizing jobs, where a strong acid (concentrated HCl) is introduced into the well to dissolve precipitated limestone, plugging the flow from the reservoir. After acidizing, production begins again and pH inside the well increases back to usual operating values, ranging mostly between 4 and 7, depending on the well. One of the main concerns with the use of stainless steels in oil and gas production is whether and under which conditions the steel can form a new passive layer, after the existing one has been dissolved.

The goal of the present paper is to investigate the limits of passivity for differently alloyed stainless steels in an artificial brine at low pH values and to study at which conditions repassivation occurs. Furthermore, it shall be determined whether there are conditions that can maintain passivity but that do not enable formation of a new passive layer in case the old one has been damaged. The exposure tests are complemented with passive layer analysis by time-of-flight secondary ion mass spectrometry (ToF-SIMS) to get a full understanding of the passivation mechanism of stainless steels at different low pH values.

2 | EXPERIMENTAL

2.1 | Materials

Seven steel grades have been investigated in this study. Table 1 shows chemical compositions and pitting resistance equivalent number (PREN, for definition see Table 1) values. Throughout this study, the investigated materials are used with the following self-explaining nomenclature (1).

XCrYNiZMo …meaning stainless steels with X wt%

Cr, Y wt% Ni and Z wt% Mo. (1)

Steels were chosen, such that a large variety in chemical composition was investigated, ranging from 13Cr up to superaustenitic stainless steel.

TABLE 1 Chemical composition and PREN values of investigated stainless steel grades

Stainless steel	C [%]	Mn [%]	S [%]	Cr [%]	Ni [%]	Mo [%]	N [%]	PREN
13Cr	0.190	0.52	0.0037	12.41	0.18	0.01	0.022	12.7
13Cr6Ni2Mo	0.013	0.36	0.0022	12.55	5.85	2.2	0.007	19.9
15Cr6Ni2Mo	0.028	0.28	0.0023	14.67	6.04	1.92	0.028	21.4
17Cr4Ni2Mo	0.033	0.33	0.0031	16.84	3.74	2.4	0.035	25.3
17Cr12Ni2Mo	0.01	1.87	0.0007	17.24	11.62	2.34	0.063	26.0
22Cr5Ni3Mo	0.027	1.79	0.0028	22.08	5.42	3.29	0.101	34.5
20Cr24Ni6Mo	0.010	0.83	0.0005	20.36	24.49	6.35	0.076	42.5

Note: PREN = %Cr + 3.3%Mo + 16·N.

Abbreviations: PREN, pitting resistance equivalent number.

The microstructure is shown in Figure 1. Whereas the lowest alloyed 13Cr steel shows a martensitic microstructure, steels 13Cr6Ni2Mo and 15Cr6Ni2Mo are bainitic. 17Cr4Ni2Mo and 17Cr12Ni2Mo steels have very similar amounts of chromium, molybdenum, and consequently PREN values (25.3 and 26.0), with only a large difference in nickel content, which affects the microstructure. 17Cr4Ni2Mo is both ferritic and bainitic, whereas 17Cr12Ni2Mo is purely austenitic. 22Cr5Ni3Mo is the only duplex steel. In Figure 1f, the ferritic phase has a gray blue color and the austenitic phase is bright. The matrix is the ferrite, which represents 55%−60% (estimated from Figure 1) of the whole microstructure. 20Cr24Ni6Mo is a superaustenitic stainless steel grade, meaning that it is austenitic in microstructure with very good corrosion resistance properties as a result of the high alloying content (superaustenites have a PREN value greater than 40). All steels show a fine grain size below 50 μm, except the superaustenite, which has a grain size of a few 100 μm. The duplex stainless steel 22Cr5Ni3Mo shows elongated grains of α- and γ-phase.

Mechanical properties are given in Table 2. Tensile specimens were made from the steels and were tested to determine the mechanical properties, namely tensile strength (R_m), yield strength ($R_{p0.2}$), fracture elongation ($A_{25\,mm}$), as well as reduction of area (Z; Table 2). The two austenitic stainless steels showed a much higher fracture elongation than the martensitic and bainitic ones. All steels have a tensile strength between 700 and 1070 MPa, a yield strength between 510 and 1020 MPa, and a reduction of area between 63% and 82%.
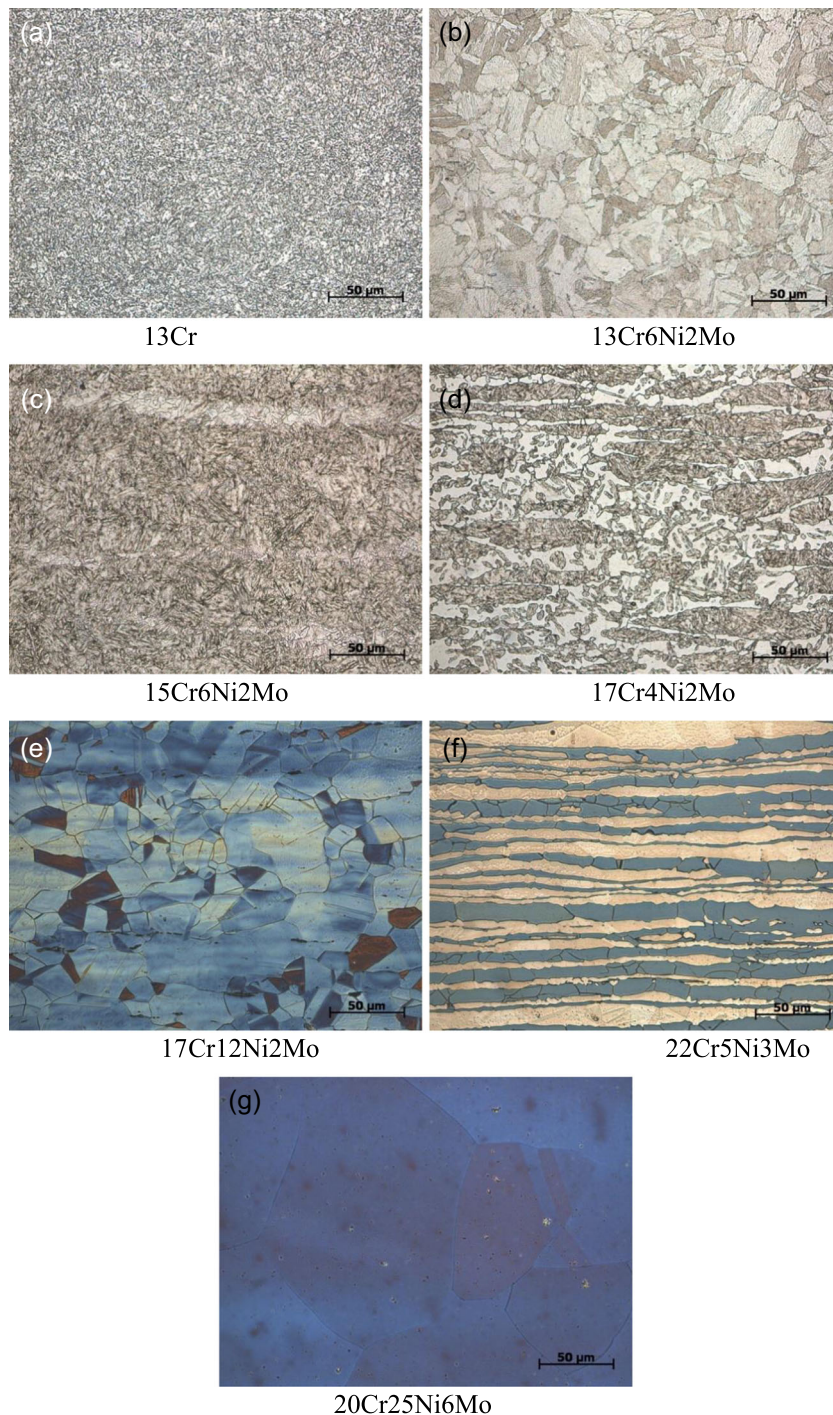
2.2 | Depassivation−repassivation test

The chemical depassivation−repassivation test (Figure 2) was developed to investigate the difference between depassivation and repassivation pH values. All tests were done at open circuit potential. The pH of the solution is decreased until the passive layer dissolves, followed by an increase of pH until repassivation occurs. Once the passive layer fails, a large amount of corrosion can be expected to occur, which will also change the composition of the solution. Therefore, it was decided to perform experiments in a flow cell. Three solution containers (one 300-L container and two 130-L containers) were used, which were filled with 5% NaCl at different, but fixed, pH values, where the pH ranged between 5 and 0, depending on the investigated steels. The pH was adjusted by the addition of concentrated HCl, which affected Cl⁻ concentration. All three solution containers were thoroughly deaerated by means of argon purging for a period of 24 h before starting the experiment, ensuring a level of dissolved oxygen between 20 and 70 ppb.

The solution was pumped from the containers using precise membrane pumps in different ratios into a mixing chamber, obtaining the desired pH value of the solution flowing into the cell. Viton tubing was used, which was immersed into a thermostated heating bath to obtain the desired temperature of the solution before it would enter the insulated flow cell. The flow cell itself was additionally purged with argon to ensure that the amount of dissolved oxygen would not increase. The pH of the solution was measured inside the flow cell before the solution reached the samples. After leaving the flow cell, the solution was pumped into a waste solution container. The flow was set to a rate of 2 L/h at a flow velocity of circa 0.3 mm/s to avoid flow effects on mass loss. The volume of the flow cell was 0.5 L, meaning that it would take 15 min to completely change the solution inside the cell.

Cylindrical steel samples with Ø = 5 mm with rubber tubing around them were placed into a 3-mm thick polytetrafluoroethylene (PTFE) sheet with holes to accommodate them. The samples were placed in such a

FIGURE 1 The microstructure of investigated materials

way that the lowest alloyed 13Cr steel was closest to the flow cell outlet, whereas the highest alloyed steel 20Cr24Ni6Mo was placed closest to the electrolyte inlet of the flow cell. This shall ensure that the dissolved metallic ions from the already corroding samples do not affect the samples that are still passive. The PTFE sheet was then placed at the bottom of large molds (60 mm × 60 mm × 60 mm), which were filled with an epoxy resin in several stages, forming sample blocks (Figure 3). Temperature for most tests was 30°C and some tests were done at 80°C.

The samples were connected to a multiplexer (34972A LXI Data Acquisition/Switch Unit; produced by Keysight[23]), measuring the potential of each sample and recording it every 15 s using a saturated calomel electrode (SCE) during 30°C tests and an Ag/AgCl reference electrode during 80°C tests. The input impedance was set for all channels greater than 10 GΩ in the same way as described by Linhardt et al.[24] In contradiction to them, a multichannel potentiostat was not available. Therefore, only potentials were recorded and no polarization resistance measurements were

TABLE 2 Mechanical properties of investigated stainless steel grades

Stainless steel	$R_{p0.2}$ [MPa]	R_m [MPa]	$A_{25\,mm}$ [%]	Z [%]
13Cr	625.9	779.4	22.1	70.3
13Cr6Ni2Mo	714.9	839.4	23.9	79.3
15Cr6Ni2Mo	1010.5	1064.0	21.6	70.7
17Cr4Ni2Mo	798.1	960.2	22.8	65.5
17Cr12Ni2Mo	521.1	709.5	47.4	77.8
22Cr5Ni3Mo	790.5	940.7	19.9	68.3
20Cr24Ni6Mo	344.1	738.2	56.9	81.8

FIGURE 3 The prototype sample block with embedded seven investigated materials (contact at backside, not visible) for simultaneous evaluation in the chemical depassivation test
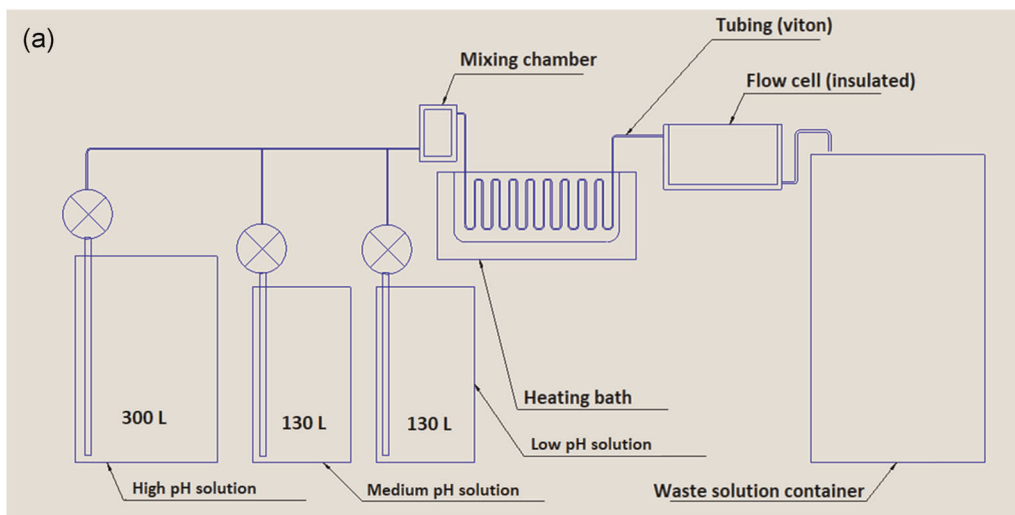

FIGURE 2 (a) A schematic of chemical depassivation test and (b) the experimental setup of the chemical depassivation test

done in this study. Before immersion, the sample blocks were wet-grinded with #2500 abrasive SiC paper, ensuring a flat and smooth surface when the samples were in contact with the solution. The oxygen probe and the pH electrode were connected to a transmitter (M200 transmitter; produced by Mettler Toledo), which logged concentration of dissolved oxygen in the largest solution tank as well as pH and temperature inside the flow cell every 15 s. Additionally, a camera was placed at the bottom of the flow cell, taking images of the exposed samples every 15 min.

The experiment involved reducing the pH inside the cell at 0.25 pH steps, followed by increasing the pH inside the cell at in 0.25 pH steps, returning to the original pH value. The sample block was exposed to the solution with a constant pH level for 12 h each (to maintain steady-state conditions). Besides the potential drop that occurs during depassivation (activation) and the potential increase obtained during repassivation, as a second indicator for the depassivation and repassivation pH values, the formation of hydrogen gas bubbles on the specimen during active corrosion was visually observed via a CCD camera. Test duration of each experiment was 204 h. After the experiment, each specimen was investigated by an optical microscope at magnifications ×10 and ×100 to check the type of attack. In all cases, uniform corrosion as a sign for depassivation of the steel was obtained, together with a significant increase of surface roughness of the depassivated steel sample and a matte gray color. No evidence of crevice corrosion was observed on the steel samples. Material loss on the specimens was several 100 μm and a pronounced step

between the original block surface on the resin and the depassivated steel surface was present.

2.3 | Scratch test

A scratch test has been performed under conditions where the passive layer can only be maintained but not rebuilt once destroyed. Two identical electrodes of the metal are used, where one is scratched via a Vickers hardness indenter. Potential of the scratched electrode was measured versus a reference electrode via a high-impedance voltmeter. Current between both steel specimens (scratched and unscratched) was measured by using a zero resistance ammeter. The experimental procedure of the scratch test is described in detail elsewhere.[14]

2.4 | ToF-SIMS analysis of passive layers

ToF-SIMS was performed with a "TOF SIMS 5" spectrometer produced by IONTOF. This method provides information about the chemical composition of the oxide depth profile as well as the depth of the oxide layer. The samples were investigated by use of a Cs^+ ion sputtering beam of 0.5-keV energy, across an area of $400 \mu m \times 400 \mu m$, and a Bi^+ ion analysis beam of 30-keV energy, scanning across an area of $100 \mu m \times 100 \mu m$. The sputtering rate of the technique is approximately 0.020 nm/s for Cr_2O_3 oxides. The original profiles measured had the time as the x-axis, and this was changed into a depth profile x-axis by
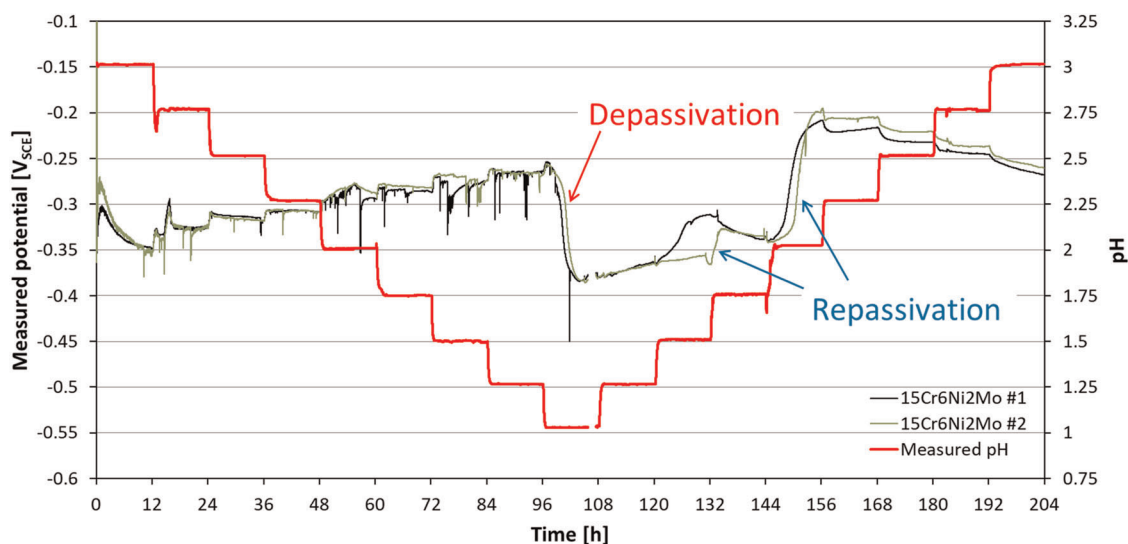

FIGURE 4 Measured potential during exposure of 15Cr6Ni2Mo steel to 5% NaCl solution at 30°C, Ar-purged
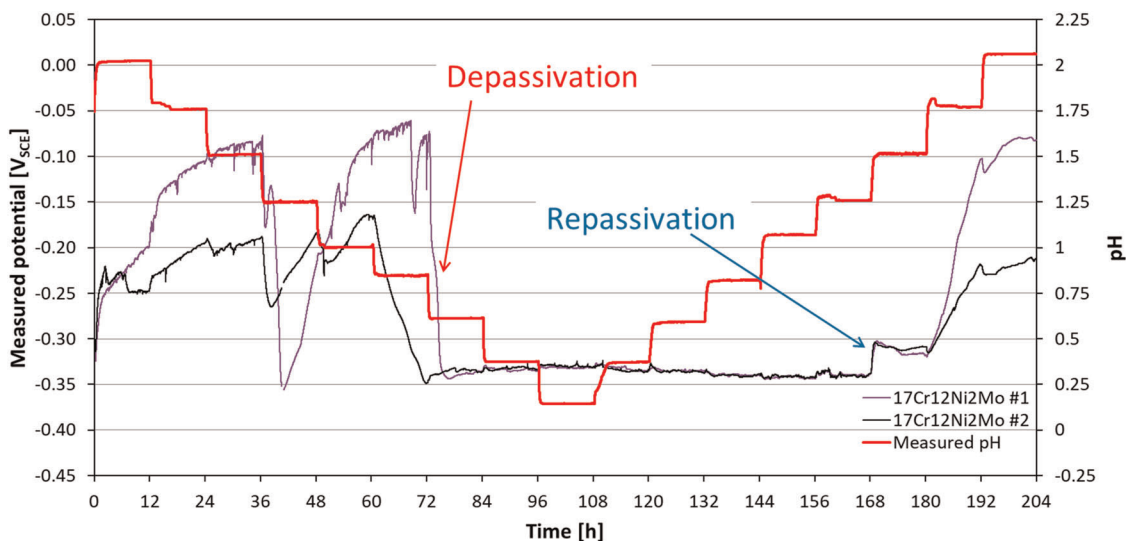
FIGURE 5 Measured potential during exposure of 17Cr12Ni2Mo steel to 5% NaCl solution at 30°C, Ar-purged

multiplying the measurement time with the sputtering rate h [nm] = 0.020 [nm/s] × t [s].

3 | RESULTS AND DISCUSSION

3.1 | Depassivation−repassivation tests

In Figures 4–7, the various possible outcomes of depassivation−repassivation tests are shown. The desired outcome of a depassivation−repassivation experiment is shown in Figure 4 for steel 15Cr6Ni2Mo. The potential decrease at pH 1 corresponds to depassivation, whereas the potential increase at pH 1.75 corresponds to repassivation. The potential increase in Sample 1 at pH 1.5

is an artefact, which appeared due to the formation of a large gas bubble covering most of the surface of the sample. The gas bubble was removed, when the pH was adjusted. The formation of gas bubbles due to hydrogen evolution agreed very well with the potential drop and increase shown in Figure 4.

Figure 5 shows the twofold depassivation process for steel 17Cr12Ni2Mo. The first is followed by an immediate repassivation. In such cases as depassivation pH, the second and final depassivation processes were considered, as hydrogen evolution during the active state was clearly obtained after the second depassivation process. During repassivation, the first increase of potential was taken according to a substantial decrease of hydrogen evolution at this stage. Sample 1 had a potential decrease, indicating
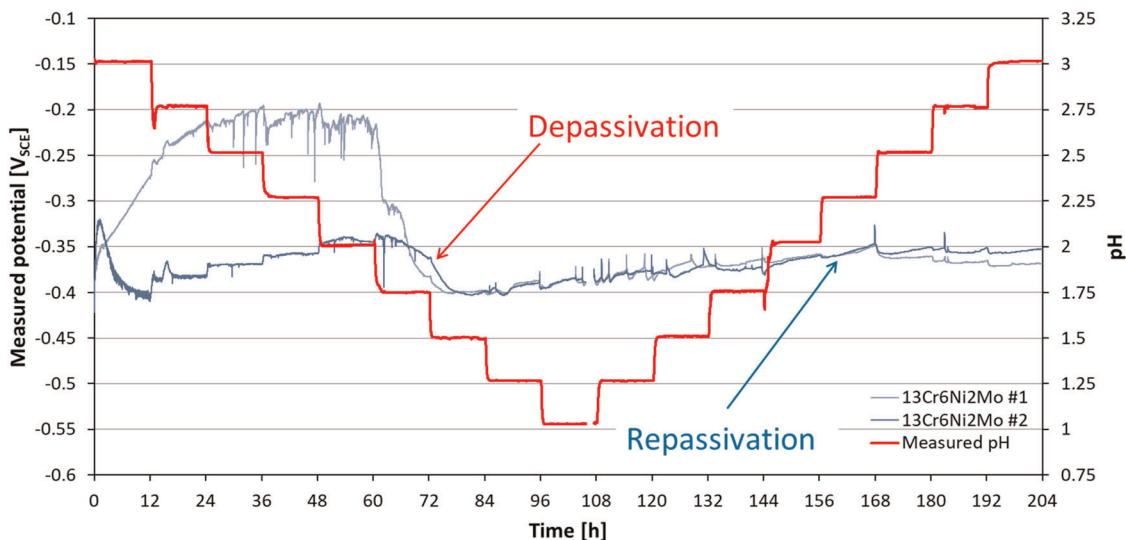

FIGURE 6 Measured potential during exposure of 13Cr6Ni2Mo steel to 5% NaCl solution at 30°C, Ar-purged
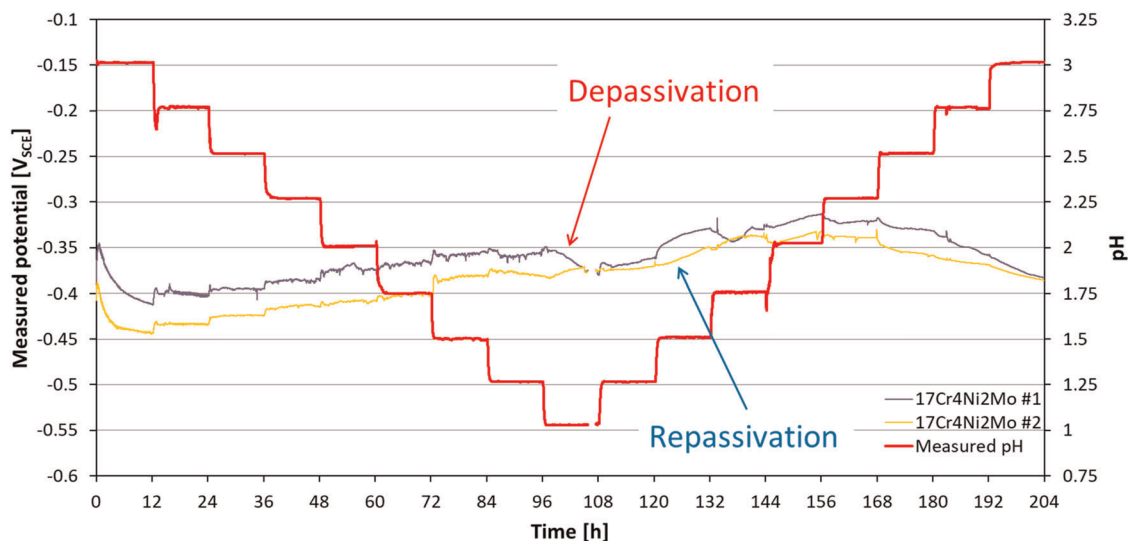
FIGURE 7 Measured potential during exposure of 17Cr4Ni2Mo steel to 5% NaCl solution at 30°C, Ar-purged

depassivation during the pH 0.75 step, whereas Sample 2 had a potential decrease, indicating depassivation during the pH 0.5 step. Both samples then followed the same potential behavior until the shift to pH 1.75, whereas the potential increase at pH 1.5 indicates repassivation. The same depassivation and repassivation pH values were confirmed by hydrogen gas formation on the surfaces of the two samples.

In a few cases, repassivation could hardly be identified by a potential increase, as shown for steel 13Cr6Ni2Mo in Figure 6. In such cases, only the end of hydrogen evolution observed by a camera was considered for determination of repassivation pH.

Finally, there were a few measurements where almost no or only very small potential steps have been obtained during depassivation and repassivation of specimens. An example is given in Figure 7 for steel 17Cr4Ni2Mo. In such cases, mainly the start of hydrogen evolution during depassivation and the end of hydrogen evolution during repassivation were taken for determination of the two interesting pH values (pH$_{depass}$ and pH$_{repass}$).

It was concluded that the visual appearance of hydrogen gas bubbles during the active range was more precise than the potential measurements shown in Figures 4–7. Therefore, the appearance and disappearance of hydrogen evolution were taken as the main basis for determination of depassivation and repassivation pH values. The results clearly indicate that the experimental setup shall be equipped in the future with a multichannel potentiostat as described by Linhardt et al.[24] to enable additional measurement of corrosion rates by determining polarization

resistance or performing electrochemical impedance spectroscopy.

The outcome of the depassivation−repassivation tests is summarized in Table 3 for 30°C and in Table 4 for 80°C. It should be noted that the change in Cl⁻ concentration may have had an impact on the depassivation/ repassivation pH values reported in Tables 3 and 4. At pH 1, the chloride concentration increases from 30,330 to 33,578 mg/L Cl⁻, which is an increase of approximately 10% and should not have a significant effect on corrosion behavior. A further pH decrease, however, has a profound effect on Cl⁻ concentration, increasing the value to 62,795 mg/L Cl⁻ at pH 0, doubling the original concentration. In regard to this, we are able to report that in previous 24-h immersion tests, the 15Cr6Ni2Mo steel has suffered from uniform corrosion in a 0.0833% NaCl

TABLE 3 pH values obtained from immersion tests and chemical depassivation tests performed at 30°C in 5% NaCl, Ar-purged

Stainless steel	pH$_{depass}$	pH$_{repass}$	ΔpH
13Cr	3.25	3.5	0.25
13Cr6Ni2Mo	1.5	2.25	0.75
15Cr6Ni2Mo	1.0	1.75	0.75
17Cr4Ni2Mo	1.0	1.5	0.50
17Cr12Ni2Mo	0.63	1.5	0.87
22Cr5Ni3Mo	0.25	0.88	0.63
20Cr24Ni6Mo	0.0	0.75	0.75

Note: depassivation pH (pH$_{depass}$), repassivation pH (pH$_{repass}$), and difference between depassivation and repassivation pH (ΔpH).

TABLE 4 Values obtained from immersion tests and chemical depassivation tests performed at 80°C

Stainless steel	pH_{depass}	pH_{repass}	ΔpH
13Cr	3	3.25	0.25
13Cr6Ni2Mo	1.5	2.5	1
15Cr6Ni2Mo	1	1.75	0.75
17Cr4Ni2Mo	1/<1	1.25/NA	0.25/NA

Note: depassivation pH (pH_{depass}), repassivation pH (pH_{repass}), and difference between depassivation and repassivation pH (ΔpH).
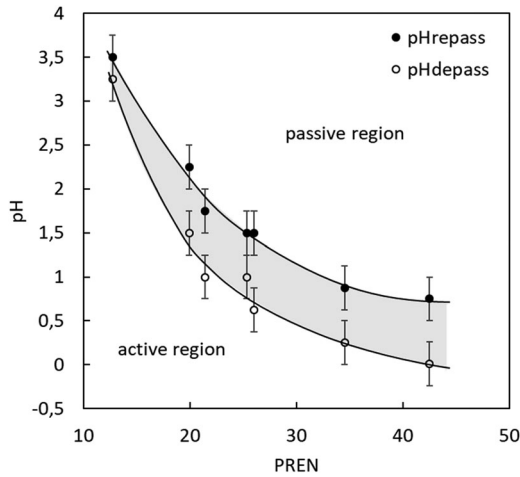

FIGURE 8 Active and passive regions in 5% NaCl at 30°C as a function of pitting resistance equivalent number (PREN); shaded area marks passivity maintaining conditions, meaning that passivity with an existing passive layer is maintained, but no new passive layer on bare alloys can be formed

solution at pH 1, which had a Cl⁻ concentration of only 3595 mg/L.[15] This result, along with the results of immersion tests performed in 5% NaCl solution as well as the results from the depassivation−repassivation tests (depassivation and uniform corrosion occur in all experiments for this steel at pH 1), clearly indicates pH value as a very important factor in depassivation conditions; however, some effect of Cl⁻ concentration on the depassivation pH value was found in immersion tests of other steels.

Figure 8 graphically shows pH values obtained at 30°C from Table 3. There is a region where the steels are actively corroding and a second region where the steels are passive. In addition, there is a shaded area in between both regions, where a passive layer, if present, can be maintained by the alloy; however, when immersing the steel in the active condition into the solution, no new passive layer can be formed. The error bars in Figure 8 are 0.25 pH units up and down from the experimentally obtained depassivation and repassivation pH corresponding to the pH step size during the experiment.

3.2 | Scratch test

A scratch test was performed on a steel in the pH region between depassivation and repassivation pH values. 13Cr6Ni2Mo steel with PREN value of 19.9 was chosen for this purpose, due to the large difference between these two pH values. Before the test, the steel electrodes were passivated for 24 h in a deaerated 5% NaCl, pH 3 solution at 30°C, followed by the addition of HCl to decrease the solution pH to 2. After pH 2 was achieved, the electrodes were left in the new solution for 4 h to reach steady-state conditions, followed by the scratch event. After scratching, the electrodes were left in the solution for an additional 24 h before removing them from the solution. After removal, ultrasonic cleaning in ethanol and investigation of the surface with an optical microscope were done. Figure 9 shows the surface of the scratched electrode, where the inside of the scratched area has become matte gray due to corrosive attack,
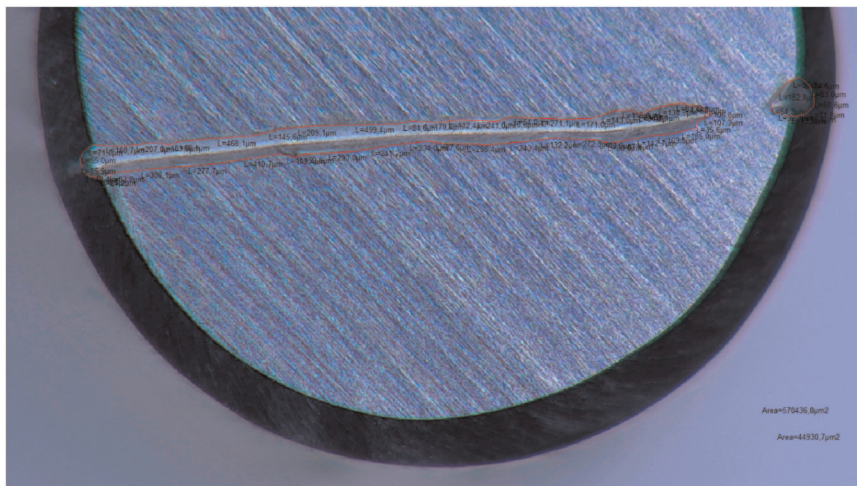

FIGURE 9 The surface of WE 1 from 13Cr6Ni2Mo steel after the scratch test in pH 2, 5% NaCl at 30°C; the scratched area has suffered uniform corrosion, whereas the rest of the electrode has remained passive

whereas the original surface still shows grinding marks and it has remained reflective, indicating that passivity was maintained there. The unscratched electrode also remained reflective with visible grinding marks.

The difference in current just before scratching and 180 s after scratching was equal to 290 nA (Figure 10), a value that increased over the next 24-h immersion (most likely due to the increase of corrosion in the affected area). Considering general corrosion in the scratched area of 0.71 mm², the calculated corrosion rate was at least 0.41 mm/y (calculated via the Faradaic law). This calculated corrosion rate is a lower limit, as no current is considered to flow from the scratched area into the unscratched area of the specimen, which, however, will always take place. Due to the distance and ohmic drop between the two steel specimens, it can be assumed that a certain amount of current flows into the cathodic (unscratched) region of the scratched specimen. A conservative way of evaluating this internal current would simply be to compare the cathodic (unscratched) areas of both electrodes, which are approximately equal, meaning that the corrosion rate inside the scratched area is at least twice the value calculated above.

This scratch test proves the existence of passivity maintaining conditions that do not enable repassivation to occur.

The most likely interpretation is that a hysteresis for a passive layer formation and dissolution exists. Figure 11 shows a passivity maintaining the pH range between the active and the passive pH region as a consequence of this hysteresis between depassivation and repassivation. In this pH range, an existing passive layer is maintained,
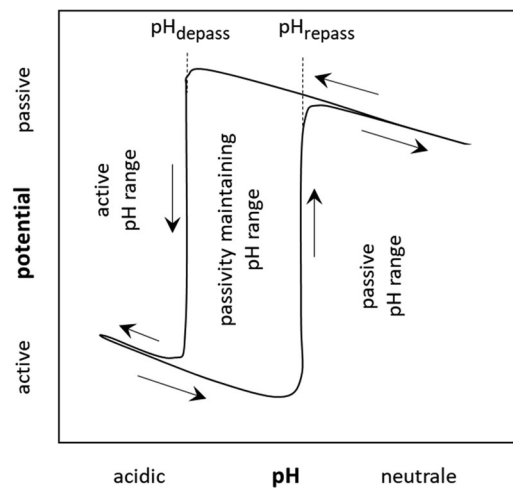

FIGURE 11 A schematic of depassivation−repassivation test results in a E-pH plot

whereas a new one cannot be formed. There is a pH value below which the alloys are active, not dependent on starting conditions (with or without passive layer). Above a certain pH value, the steels are passive, again independent of starting conditions. In between both states, there is a pH range where the state depends on starting conditions of the surface. An active surface will remain active, a passive one will stay passive. The width of this passivity maintaining conditions is dependent on the steel and on other conditions such as temperature. The experiment could not be reproduced in an aerated solution, indicating that a higher amount of dissolved oxygen stabilizes the passive state.
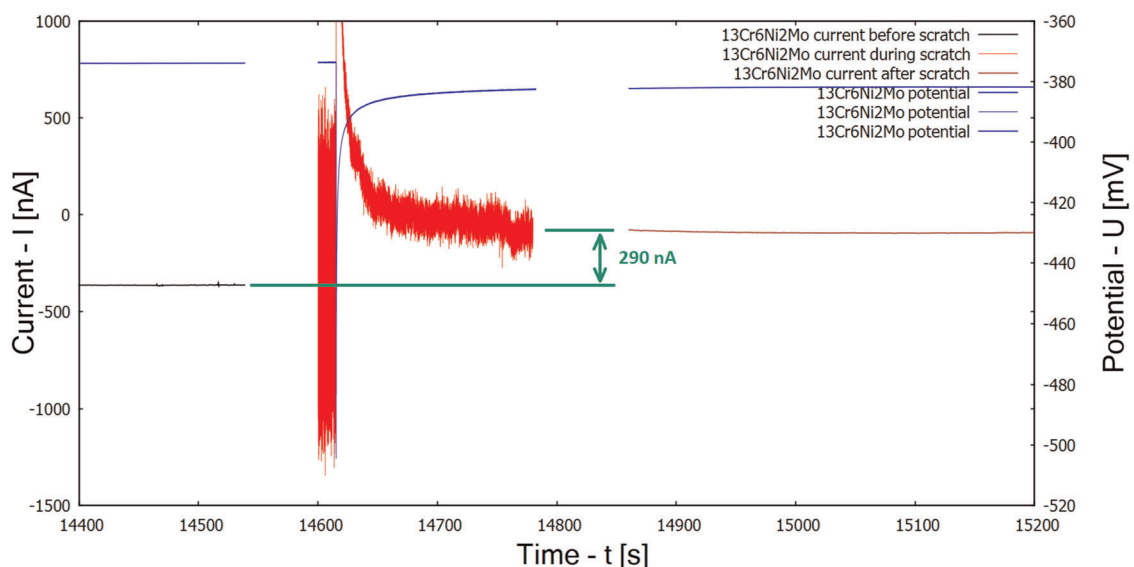

FIGURE 10 Current measurement before, during, and after scratch event confirms a current change of 290 nA between the two working electrodes
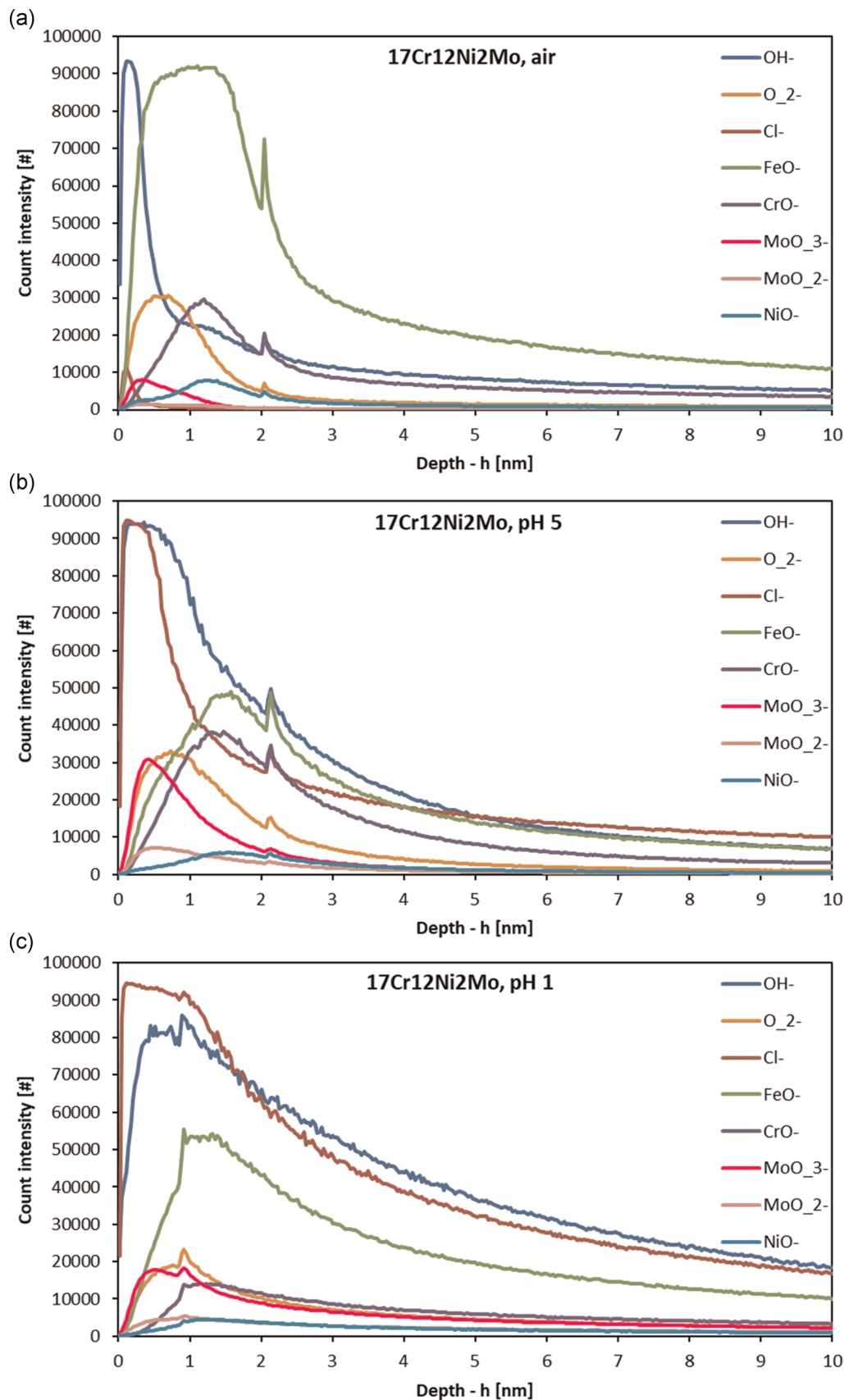
FIGURE 12   Secondary ion mass spectrometry depth profile on 17Cr12Ni2Mo steel after 24-h exposure to (a) air, (b) 5% NaCl, pH 5 solution, at 30°C, and (c) 5% NaCl, pH 1 solution, at 30°C

In the present scratch test, the passive layer on 13Cr6Ni2Mo material persisted for a period of 28 h in a deaerated 5% NaCl, pH 2 solution at 30°C. Most steels in the chemical depassivation−repassivation tests have resulted in appearance of uniform corrosion within 1−6 h after achieving the depassivation pH. As even the area adjacent to the scratched area has not been depassivated in the scratch test (where spreading of the corrosive attack could be expected) and the 13Cr6Ni2Mo steel withstood a pH between repassivation and depassivation pH values in the depassivation−repassivation tests for 36 h without producing H_2 gas on the surface, it is reasonable to expect that this steel might avoid general depassivation in such a solution indefinitely. The chloride concentration in this test was increased by less than 1%, which was considered negligible.

3.3 | ToF-SIMS analysis of passive layers

The ToF-SIMS analyses performed on the three samples of steel 17Cr12Ni2Mo have provided depth profiles of several different anions. The passive layer of this steel has been analyzed in air, in a moderate aggressive electrolyte at pH 5 that can form a passive layer, and in a highly aggressive electrolyte at pH 1 that only can maintain a passive layer. To determine the thickness of the passive layers, a sum of FeO^-, CrO^-, MoO_3^-, MoO_2^-, NiO^-, OH^-, and O^{2-} anion counts was examined. The point where the sum of all the abovementioned anion counts was reduced to 50% of their maximum value was taken to determine the location of the interface between the passive film and the underlying metal and the passive layer thickness as such. The thickness of the passive layer on 17Cr12Ni2Mo was defined by depth profiling using ToF-SIMS analysis. The passive layer formed in air is 2.6-nm thick, whereas the passive film that

formed during 24-h exposure to 5% NaCl and 30°C at pH 5 and pH 1 is 2.6 and 3.3-nm thick, respectively.

Figure 12a shows the ToF-SIMS depth profiles obtained from the stainless steel 17Cr12Ni2Mo exposed to air at room temperature. A large intensity of FeO^- was found across the entire passive layer thickness. CrO^- ions were depleted at the film surface and were somewhat present deeper in the film. Mo was also found at small intensities close to the outer parts of the passive film formed in air. Small amounts of Cl^- were found near the surface, which was attributed to contamination during sample handling. Figure 12b shows the ToF-SIMS depth profiles obtained from 17Cr12Ni2Mo sample exposed to pH 5 solution. Compared with air-passivated samples, there is a strong depletion of FeO^-. The surface was particularly depleted of this anion; however, a decrease in the count intensity is also noticeable deeper in the film. CrO^- ion count intensity is increased, and approximately 50% more ions are found across the depth of the film in comparison to the film formed in air. A large amount of Cl^- ions is found at the surface of the passive films, which was expected considering the large chloride content of the medium used during exposure. MoO_3^- and MoO_2^- counts are markedly higher after exposure to pH 5 solution, when compared with the passive layer formed in air. The depth profile of the 17Cr12Ni2Mo sample exposed to pH 1 is presented in Figure 12c. In this case, one can see a large penetration of Cl^- ions into the passive film and an enrichment of MoO_3^- and MoO_2^- ions in the layer. Compared with the exposure of the same material in pH 5 solution, a depletion of CrO^- and an enrichment of FeO^- along with an increase of the passive layer thickness are obtained.

Figure 13 shows the depth profiles of ratios between CrO^- and FeO^- across the investigated samples for 17Cr12Ni2Mo samples after exposure to different pH
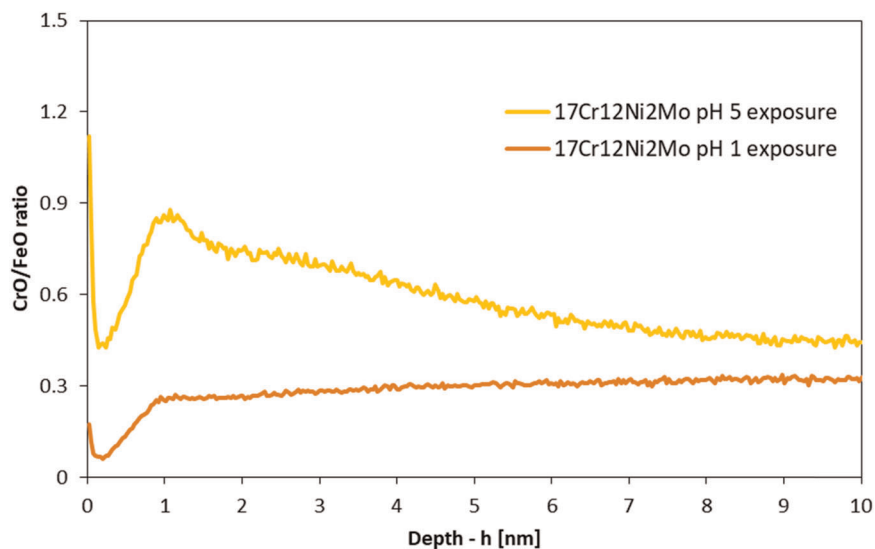

FIGURE 13 CrO^-/FeO^- ratio profiles obtained from 17Cr12Ni2Mo steel samples after 24-h exposure to 5% NaCl, pH 5 and pH 1 solutions at 30°C

solutions. The passive layer formed in pH 1 solution contains a strong chromium depletion and is not comparable to a passive layer formed in pH 5 solution.

ToF-SIMS depth profiles show that in air, there exist an inner and an outer layer of hydroxides and oxides of Fe and Cr, with CrO^- being dominant at the inner passive layer and FeO^- being dominant at the outer surface layer. When exposing the steel to an electrolyte with pH 5, Cl^- ions' content increases and FeO^- dissolves. Similar results have been found by Holzleitner.[25] When decreasing the pH to 1 preferably, Cr is again depleted and an FeO^-/MoO_X^--rich layer is formed. Results indicate that in a passive layer maintaining solution, the main constituent of the normal passive layer, CrO^-, is selectively dissolved and a layer with a larger thickness and, therefore, obviously higher defect density remains on the surface.

4 | CONCLUSIONS

The results of the present study can be summarized as follows:

− For all tested steels, cetain conditions exist, whereby passivity can be maintained but repassivation is not possible. In fact, higher alloyed steels with a higher PREN value seem to have a larger difference between the pH at which depassivation occurs and the pH at which repassivation can occur; however, other factors such as carbon content and/or microstructure, the temperature of the electrolyte, chloride concentration, and oxygen presence may also have an effect on these values.

− The difference between depassivation pH and repassivation pH is equal to or smaller than 1 pH unit and the depassivation pH was always lower than 3.5 (for 13Cr). This means that after acidizing jobs in oil and gas production, repassivation can be expected in deaerated conditions as soon as pH rises above $pH_{re\text{-}pass}$, as shown in this study.

− ToF-SIMS analysis showed that when the stainless steel comes close to its chemical depassivation limit, structure changes and the thickness of the passive layer increase. Otherwise, passive layers have a thickness of approximately 2 nm. They show an Fe-rich outer sublayer and a Cr-rich inner sublayer. When put into a somewhat aggressive electrolyte (such as brine with a pH value of 5), iron species dissolve from the surface of the passive film. In an aggressive electrolyte where the passive layer cannot be rebuilt, chromium species instead are dissolved, resulting in a thicker layer, presumably with a higher defect density. This layer is rich in molybdenum and iron oxides/hydroxides.

ORCID

Tadeja Kosec http://orcid.org/0000-0001-6790-1880
Gregor Mori http://orcid.org/0000-0001-7102-7129

REFERENCES

[1] P. Schmuki, *J. Solid State Electrochem.* **2002**, *6*, 145.
[2] C.-O. A. Olsson, D. Landolt, *Electrochim. Acta* **2003**, *48*, 1093.
[3] W. Khalil, S. Haupt, H.-H. Strehblow, *Mater. Corros.* **1985**, *36*, 16.
[4] G. Mori, R. Sonnleitner, S. Holzleitner, M. Panzenböck, R. Pippan, *Mater. Test.* **2010**, *52*, 42.
[5] M. Pourbaix, *Atlas of Electrochemical Equilibria in Aqueous Solutions*, National Association of Corrosion Engineers, Houston, TX **1974**.
[6] A. Atrens, *J. Electrochem. Soc.* **1997**, *144*, 3697.
[7] Z. Szklarska-Smialowska, *Pitting and Crevice Corrosion*, NACE International, Houston, TX **2005**.
[8] J. M. Kolotyrkin, *Corrosion* **1963**, *19*, 261t.
[9] Z. Szklarska-Smialowska, *Corrosion* **1963**, *27*, 223.
[10] M. Henthorne, in *Localized Corrosion—Cause of Metal Failure* (Ed: A. Bond), ASTM International, Philadelphia, PA **1972**, p. 250.
[11] G. S. Frankel, *J. Electrochem. Soc.* **1998**, *145*, 2186.
[12] J. Soltis, *Corros. Sci.* **2015**, *90*, 5.
[13] B. Zhang, X. L. Ma, *J. Mat. Sci. Technol.* **2019**, *35*, 1455.
[14] E. Mujanović, B. Zajec, T. Kosec, A. Legat, S. Hönig, G. Zehethofer, G. Mori, *Materials* **2019**, *12*, 3811.
[15] E. Mujanović, *Ph.D. Thesis*, Montanuniversität Leoben (Austria) **2020**.
[16] H. S. Kwon, E. A. Cho, K. A. Yeom, *Corrosion* **2000**, *56*, 32.
[17] M. Stern, *J. Electrochem. Soc.* **1959**, *106*, 376.
[18] E. A. Cho, C. K. Kim, J. S. Kim, H. S. Kwon, *Electrochim. Acta* **2000**, *45*, 1933.
[19] J.-B. Lee, *Mater. Chem. Phys.* **2006**, *99*, 224.
[20] R. Carranza, J. Galvele, *Corros. Sci.* **1988**, *28*, 233.
[21] G. T. Burstein, K. Sasaki, *J. Electrochem. Soc.* **2001**, *148*, B282.
[22] G. T. Burstein, B. T. Daymond, *Corros. Sci.* **2009**, *51*, 2249.
[23] *Keysight 34970A/34972A Data Acquisition/Switch Unit User's Guide*, Keysight Technologies, 2014.
[24] P. Linhardt, S. Kührer, G. Ball, M. V. Biezma, *Mater. Corros.* **2018**, *69*, 358.
[25] S. Holzleitner, *Ph.D. Thesis*, Montanuniversität Leoben (Austria) **2008**.